Time resolved screening of the piezoelectric field in InGaAs/GaAs V-shaped quantum wires of variable profile

1999 J. Phys.: Condens. Matter 11 5989

(http://iopscience.iop.org/0953-8984/11/31/307)

J. Phys.: Condens. Matter **11** (1999) 5989–5997. Printed in the UK PII: S0953-8984(99)01410-1

Time resolved screening of the piezoelectric field in InGaAs/GaAs V-shaped quantum wires of variable profile

M Lomascolo†§, R Rinaldi†, A Passaseo†, M De Vittorio†, M De Giorgi†, R Cingolani†, L De Caro‡, L Tapfer‡, A Taurino§ and M Catalano§

† Istituto Nazionale per la Fisica della Materia, Unità di Lecce, Dipartimento di Ingegneria dell'Innovazione, Université di Lecce, via per Arnesano, I-73100 Lecce, Italy

‡ PASTIS-CNRSM, Centro Nazionale per la Ricerca e lo Sviluppo dei Materiali, SS 7 'Appia' Km 712, 72100 Brindisi, Italy

§ CNR-IME Istituto per lo studio di nuovi Materiali per l'Elettronica, via per Arnesano, I-73100 Lecce, Italy

Received 29 January 1999, in final form 20 April 1999

Abstract. InGaAs/GaAs V-shaped quantum wires grown in grooves with either (111) or (411) sidewalls have been studied by ps-transient photoluminescence as a function of the excitation intensity. The optical nonlinearity associated with the screening of the internal piezoelectric field is temporally monitored by the blue-shift of the spectrally resolved photoluminescence, occurring in the first 150 ps after the laser pulse, followed by the recovery of the unperturbed energy resonance at longer delays. Such an energy shift strongly depends on the photoexcited carrier density and reaches a maximum value of about 14 meV in the (411) wires. Despite their larger piezoelectric field, we observe a smaller energy shift in wires with (111) sidewalls, due to the enhanced confinement which localizes the wire wave-function at the bottom of the groove. The observed energy shifts are consistent with the theoretical calculation of the polarization charge density induced by the strain via the piezoelectric effect.

1. Introduction

Zincblende heterostructures grown along crystallographic directions other than (001) present a large piezoelectric activity [1]. The polarization charge density induced by the strain at the high index interfaces modifies the energy band structure and renormalizes the exciton levels by shifting the resonance to lower energy through the quantum confined Stark effect [2–4]. Strained InGaAs based quantum wells (QWs) and quantum wires (QWRs) thus become quite interesting for the design of new structures exploiting the tailored strength and orientation of the piezoelectric field [5]. These structures have improved electronic characteristics such as high mobility, and enhanced optical nonlinearity induced by the screening of the internal piezoelectric field by the external perturbations (either electric or electromagnetic fields [6–10]). Beside their fundamental interest, these effects are relevant for future applications to optical devices such as modulators and optical switches based on InGaAs nanostructures. In this work we present a systematic investigation of the transient photoluminescence (TPL) in strained InGaAs/GaAs V-shaped QWRs grown in grooves with different crystallographic orientation of the sidewalls ((411) and (111)), as a function of carrier density. The screening of the internal piezoelectric field manifests itself by the blue-shift of the photoluminescence in the first 150 ps after the laser pulse, followed by the recovery of the unperturbed energy resonance at longer delays. Such an energy shift strongly depends on the sidewall orientation and on

0953-8984/99/315989+09$30.00

the photo-generated carrier density, which is tuned in the range 10^9–10^{12} cm^{-2}, i.e. close to the polarization charge density. The screening induced blue-shift saturates at the maximum value of about 14 meV, when the carrier density exceeds 3×10^{11} cm^{-2} in wires with (411) oriented sidewalls. On the other hand, wires with (111) oriented sidewalls, which should exhibit a much larger piezoelectric potential, show a reduced screening induced shift due to the enhanced confinement which localizes the wave-functions at the bottom of the groove, where the strength of the piezoelectric field approaches zero.

2. Experiment

The investigated QWRs were fabricated by metal–organic chemical vapour deposition (MOCVD) of a single 3 nm $In_{0.1}Ga_{0.9}As$ quantum well (QW) on patterned V-grooved GaAs substrates. The patterned substrates were realized by holographic photolithography and wet chemical etching with typical periodicity of 500 nm. A proper control of the anisotropic etching process resulted in two different groove profiles and, in turn, wire shapes. The usual crescent-shape wires self-organize at the bottom of the grooves with (111) wires, whereas a constant thickness wire forms at the bottom of the grooves with (411) wires. Transmission electron microscopy images clearly reveal the crystallographic planes at the InGaAs/GaAs interfaces, the different angles at the apex of the wires, and the tapering of the InGaAs thickness in the two structures (figures 1(a) and 2(a)). The (411) wires (figure 2(a)) lie on (411) surfaces and exhibit a constant thickness along the sidewalls of (3.5 ± 0.3) nm (i.e. close to the nominal thickness of the reference planar quantum well). In this case the bending angle is $(139 \pm 3^\circ)$ and the lateral confinement primarily arises from the QW bending and from the weak planarization occurring at the bottom. In the case of the (111) quantum wires (figure 1(a)), the sidewalls lie on the (111) surfaces, whereas the tapered part of the wire stands at the bottom of the groove and is limited by (322), (311) and (100) planes at the bottom interface (GaAs/InGaAs) and by (311) and (100) planes at the top interface (InGaAs/GaAs). The well thickness at the apex of the wire is (9.4 ± 0.4) nm and the lateral dimension of the tapered region is (58 ± 2) nm. In this case the lateral confinement arises primarily from the tapering of the QW thickness and from the narrower bending angle of the wire (about 90°) [11].

The TEM pictures allow us to determine the actual shape of the nanostructures along the x (the lateral distance from the bottom of the groove) and the z (the growth direction) axes. This is shown by the straight lines in figure 1(b) and figure 2(b) for the (111) and (411) oriented sidewalls respectively. From these profiles we obtain the two dimensional confinement potential $V(x, z)$ in the cross section of the structure. This is done by mapping the energy gap of the sample in the two dimensional (x, z) array of figure 1(b) and figure 2(b). The contour plots represent the theoretical electron ground level wave function, obtained by expanding the envelope function in terms of the solution of the rectangular wire with infinite barriers and solving the Schroedinger equation for the potential $V(x, z)$ [12]. The transverse extension of the ground level wave function is found to be about 40 nm for the (411) wires and 20 nm for the (111) wires. The respective confinement energies amount to 5 meV and 12 meV for the two structures [13, 14].

Time resolved photoluminescence experiments were performed by using a Ti:sapphire mode locked laser delivering 2 ps pulses at 82 MHz repetition rate. The excitation wavelength was fixed at 800 nm, resulting in e–h pairs with excess energy about two GaAs LO phonons (36 meV) above the ground level. The integrated excitation power ranged between 1 and 280 mW under weak focalization. Assuming a carrier capture efficiency into the wire equal to unity, an absorption coefficient of 10^4 cm^{-1} and a reflectivity of 30%, we estimated the *upper limit* for the photo-generated carrier density in the wire to be equivalent to 2×10^9 cm^{-2} per

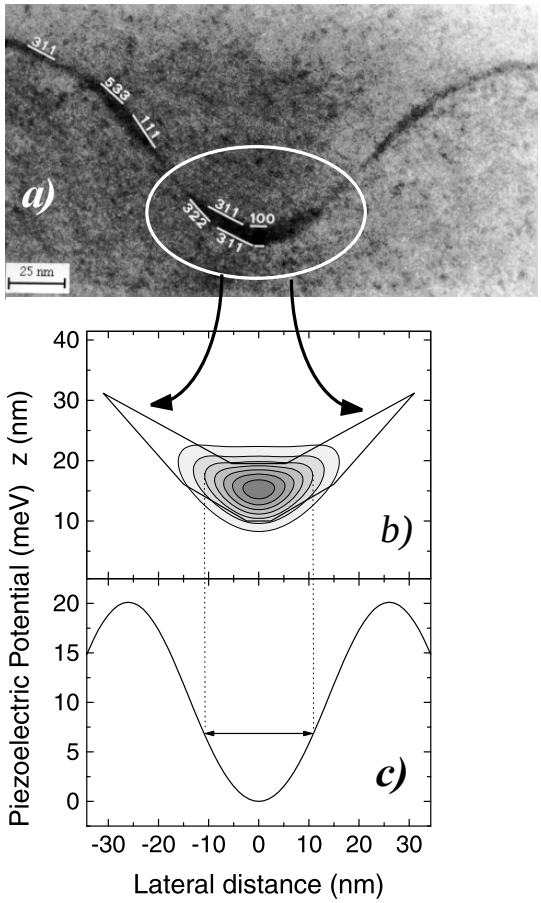

Figure 1. (a) [$0\bar{1}1$] cross sectional, low magnification high resolution image of a (111) sidewall quantum wire. (b) Contour plot representing the theoretical electron ground level wave function. (c) Piezoelectric potential generated in the quantum wires as a function of the lateral distance from the bottom of the wire. The horizontal arrow indicates the lateral extension of the ground level wave functions (see text).

mW of integrated power. The luminescence was dispersed by a 0.24 m single monochromator coupled with a streak camera operating in synchroscan mode, equipped with a two dimensional CCD. The system provided an overall time resolution of about 20 ps and an energy resolution of about 2 meV. The samples were mounted on the cold finger of a closed cycle He cryostat at a temperature of 20 K

3. Results

In figures 3(a) and 3(b) we plot the typical PL spectra of a (411) sample recorded at increasing delays after the laser pulse. The measurements were performed at intermediate photo-generation rates (about 1×10^{11} cm^{-2}). In figure 3(a) we show the spectra recorded in the first 130 ps, corresponding to the rise of the quantum wire photoluminescence centred at about 1.475 eV. This transient corresponds to the time needed for the build-up of the electron hole plasma in the wire, which is primarily governed by the capture time of the photo-generated

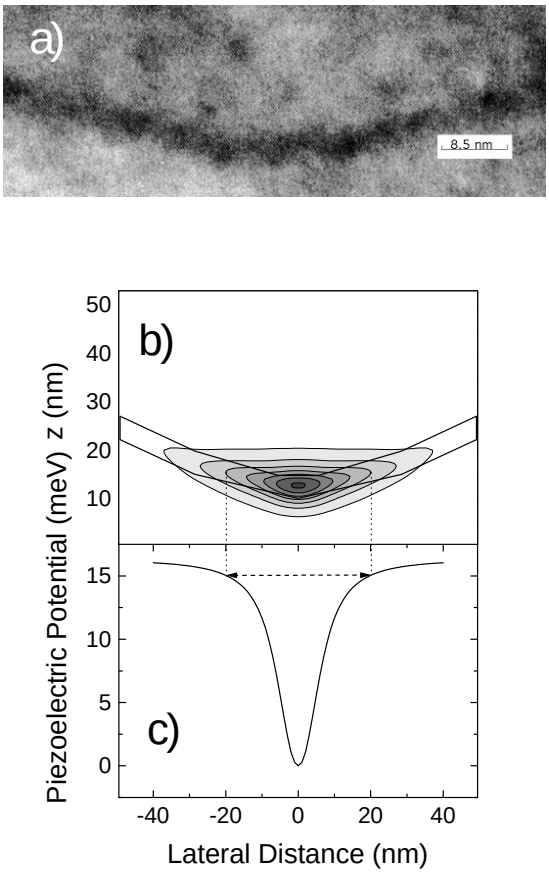

Figure 2. The same as in figure 1, for a (411) sidewall quantum wire.

carriers diffusing from the GaAs barrier into the QWRs.

The most important feature observed in these spectra is the quite large blue-shift of the QWR emission with increasing delays (of the order of about 10 meV in this case). This is a clear manifestation of the transient screening of the piezoelectric field [9, 10, 15–17] which is enhanced as long as the density of carriers in the wire is increased by relaxation and capture. In other words, due to the existence of a strong electric field along the wire structure, the electron–hole plasma during its relaxation comes to be polarized in the confining potential, resulting in a electric field which opposes the internal piezoelectric field [9, 10].

The traces recorded in the following 3 ns (from 195 ps to 3240 ps after the laser pulse) are plotted in figure 3(b). The GaAs component of the PL spectra lies at 1.515 eV and decays with a time constant of about 500 ps. On the other hand the component arising from the QWRs undergoes a red-shift which compensates the blue-shift observed at short delays. This behaviour is due to the progressive reduction of carriers in the wire, induced by recombination, which causes the reduction of screening and the recovery of the built-in piezoelectric field.

For delays longer than 500 ps two slow components are also observable in all samples. The first lies about 36 meV below the wire resonance, being associated with one GaAs LO phonon assisted emission. The second is centred around 1.493 eV, and is assigned to carbon related impurities.

In order to study the role of the (100) and (411) QW in the recombination dynamics, we

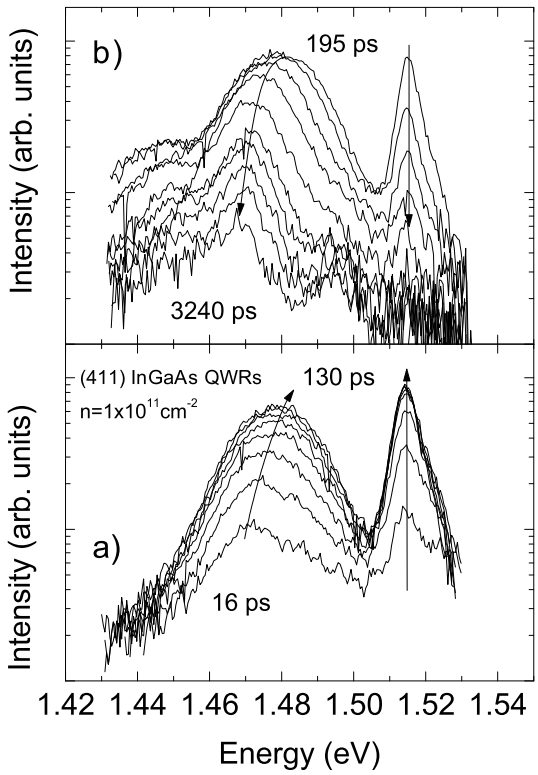

Figure 3. (a) Low temperature (20 K) PL spectra recorded at increasing delays (approximately every 15 ps) after the laser pulse in the first 130 ps for a quantum wire with a (411) sidewall. The photo-generated carrier density is about 1×10^{11} cm^{-2}. The blue-shift of 12 meV in the QWRs resonance at 1.470 eV is induced by the screening of the piezoelectric field. (b) PL spectra recorded in the same sample at longer delays (approximately every 325 ps for 3 ns). The recovery of the unscreened level is due to carrier recombination and to the progressive depletion of charge inside the wire (see text).

performed time resolved PL with higher spectral resolution though with a limited temporal window (about 1200 ps) and a lower time resolution. This is shown in figure 4, where we compare (on linear scale) a few selected transient spectra at high and low excitation (figures 4(a), 4(b) respectively).

In the high excitation spectra one can see the planar QW emission at 1.478 eV, having a decay time of $\tau = 570$ ps, which does not exhibit any shift in time, as expected for the (100) oriented growth direction. The (411) QW is observed during the first 340 ps at energy about 8 meV higher than the planar (100) QW, in reasonable agreement with the position calculated including strain and thickness deduced from the TEM images [18]. The energy shift of the (411) QW is not resolved due to its fast recombination ($\tau \approx 50$ ps). This is consistent with the high scattering rate of the lateral (411) QW into the quantum wires, the probability of the scattering being linearly dependent on the overlap integral between the two states. The blue-shift of the QWRs resonance (about 2.5 meV in the range 50–120 ps) and the subsequent red-shift (about 6 meV in the range 120–1050 ps) are perfectly consistent with the spectra of figure 3(a), (b) recorded with higher time resolution with similar excitation intensity ($n = 1 \times 10^{11}$ cm^{-2}). On the other hand at low injection rates the QWRs resonance stays fixed at about 1.463 eV (figure 4(b)). Its decay time depends on the excitation intensity and in

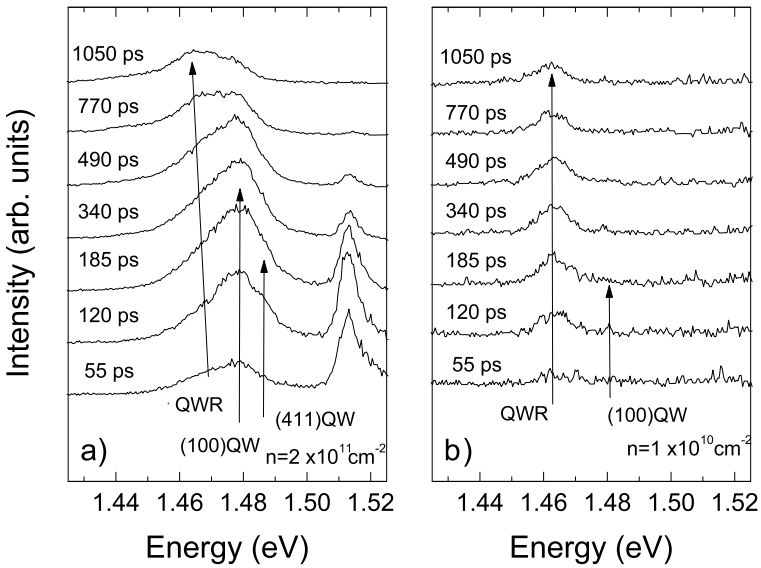

Figure 4. High spectral resolution PL spectra recorded at different not evenly spaced delays after the laser pulse, of (411) wires under high (a) and low (b) excitation intensity.

the high excitation regime is of about 1500 ps.

Finally, we note that both the planar QW and the QWR emissions exhibit the same rise time of about 150 ps. This rules out the possibility that the observed blue-shift originates from the filling of the QW states in delays after the laser pulse. In this case a longer rise time should in fact be observed for the QW resonance. Furthermore we still observe the recovery of the unperturbed QWRs resonance at long delay times, when the (411) QW and the (100) QW have disappeared from the spectra.

Figure 5(a) exemplifies the density dependence of the transient screening in both the (411) (closed symbols) and (111) samples (open symbols). The transient PL shift changes dramatically both with the excitation intensity, tuned in the range 2×10^{10}–4×10^{11} cm^{-2}, and with the sidewall orientation. The (411) wires exhibit a strong density dependence. At low photo-excited carrier densities (full triangles) no relevant shift is observed during the first 1000 ps (less than 2 meV, comparable to the resolution of our experiment), indicating that the photo-generated charge density is not enough to cause screening of the piezoelectric field. With increasing photo-excited carrier density (full dots) we observe a progressive increase of the PL blue-shift in the first 150 ps, which reflects the screening of the polarization charge induced by the photo-excited carriers relaxing from the GaAs barrier into the wire level. A 'quasi-instantaneous' screening effect is observed in the first 20 ps, due to the partial fast relaxation (below our system resolution) of carriers into the wire by LO phonon interaction. With increasing excitation intensity (full squares) the blue-shift saturates to the maximum value of 14 meV. For delays longer than 200 ps the unscreened energy level is recovered in about 1 ns, consistent with the carrier reduction induced by recombination.

A further red-shift of about 4 meV below the ground level is observed at very low excitation intensity for time delays longer than 1 ns, probably due to carrier localization at interface or compositional fluctuations. This effect becomes observable when the carrier density is low

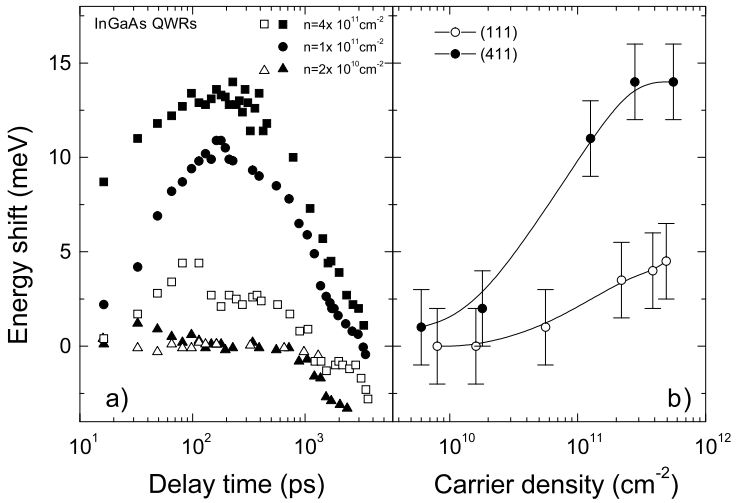

Figure 5. (a) Time evolution of the energy shift of the PL peaks for different excitation intensities in the (411) and (111) samples (closed and open symbols respectively). (b) Density dependence of the screening induced shift of the quantum wire emission (taken after 150 ps) for the (411) and (111) wires. The curves are guides for the eye. The saturation value of about 14 meV occurs for carrier density above 2×10^{11} cm^{-2} for the (411) sample, and above 5×10^{11} cm^{-2} for the (111) one.

enough to prevent saturation of the localization centres. The localization energy in these systems is expected to be few meV [11, 19]. It is worth noting that the same analysis has been performed on the reference (001) quantum well. No PL shift is observed over the first ns, whereas a weak localization induced red-shift is seen at longer delays.

The QWRs with (111) sidewalls exhibit a much weaker dynamics with increasing excitation density (open symbols in figure 5(a)). The saturation value of the blue-shift is indeed one-third of that observed in the (411) samples at the maximum injection rate (empty squares). The density dependence of the screening induced shift for both the (411) and (111) wires is better summarized in figure 5(b) where we plot the maximum shift reached at fixed delay of about 150 ps versus the carrier densities. The blue-shift of the PL reaches about 14 and 5 meV in the (411) and (111) structures, respectively. It is worth noting that, even though the internal piezoelectric field is expected to be stronger in the (111) wires, the enhanced confinement potential partially compensates the screening of the piezoelectric field, and the observed blue-shift is considerably reduced as compared to the (411) wires. In particular, we expected that the larger confinement potential of the (111) wires localizes carriers at the bottom of the groove, close to the (001) interface, where the strength of the piezoelectric field (and consequently the energy correction due to the quantum confined Stark effect) approaches zero.

4. Discussion

In order to obtain a quantitative analysis of the observed optical nonlinearity, and to describe the different behaviour depending on the groove orientation, we calculated the strain induced piezoelectric field in the two heterostructures. Assuming that the quantum wire profile can be described by a smooth function $z(x)$, in a small neighbourhood of an arbitrary point $(x, z(x))$ of any heterointerface, we can approximate the curve $z(x)$ with its tangent at that point $t(x, z(x))$.

Thus, we locally approximate the actual heterointerface profile with a linear one, which is oriented along the arbitrary direction $n(x, z(x))$, where $n(x, z(x))$ is the normal to $t(x, z(x))$ at point $(x, z(x))$. Details about the schematic diagram and the geometrical meaning of the functions $z(x)$, $n(x, z(x))$ and $t(x, z(x))$ can be found in [20] and [21].

Assuming that the heterostructure is coherent and the thickness of the barrier is much greater than the quantum-wire thickness, we can evaluate the local elastic strain field ε_{ij} of the structure by using the elasticity theory for a plane coherent heterointerface of arbitrary crystallographic orientation [20, 21].

The local elastic strain field induces a piezoelectric polarization field which is given by: $\boldsymbol{P}_{i'}(x) = 2e_{14}\varepsilon_{j'k'}(x)$, with $i' \neq j' \neq k'$, where e_{14} is the piezoelectric constant. The piezoelectric polarization induces a fixed volume charge density $\rho(x, z) = -\boldsymbol{\nabla} \cdot \boldsymbol{P}$ and a fixed interface charge density $\sigma(x) = \pm \boldsymbol{P}(x) \cdot \boldsymbol{n}(x, z(x))$ which generates a spatially varying potential across the structure. This piezoelectric field influences the transition energies via the Stark effect. It turns out that, at the bottom of the groove, the piezoelectric polarization charge is equal to zero, whereas it increases with increasing the lateral distance from the centre. If we take into account the actual wire profile as obtained by the TEM analysis, we obtain the piezoelectric potential versus the lateral distance (from the bottom of the groove) plotted in figures 1(c) and 2(c) for the (111) and (411) wire respectively. As discussed in section 2, the (411) wire has an almost constant thickness (3 nm), for any lateral distance from the centre. In contrast, the (111) wire thickness is maximum at the groove centre (where the polarization charges are missing), and reduces to less than 2 nm far from the centre (where the density of polarization charge is quite large). The constant thickness of the (411) wire causes a quick increase of the piezoelectric potential which saturates to the value of 15 meV in about 30 nm (figure 2(c)). On the other hand the piezoelectric potential profile in the case of the wire with (111) sidewalls is found to be deeper and wider (figure 1(c)). This is due to the smoothed geometrical profile of the wire at the bottom of the groove (whose surface is close to the (001) plane for about 7 nm), and to the thickness reduction at larger lateral distances (see figure 1(a)). For larger lateral distances the piezoelectric potential increases substantially due to the enhanced piezoelectric effect in the (111) direction, reaching a maximum value of 20 meV about 26 nm far from the centre of the wire. Then it decreases due to the progressive decrease of the InGaAs layer thickness (from 9 nm to about 2 nm) occurring on the lateral sidewalls of the wire, which reduces the strength of the piezoelectric field.

However, due to the different lateral extensions of the wave functions in the (411) and (111) QWRs, schematically indicated by horizontal arrows in figures 1(c) and 2(c), the values of the piezoelectric field that the carriers experience in the wires are very different for the two cases: about 4.5×10^6 V m^{-1} for the (411) wire and 0.5×10^6 V m^{-1} for the (111) wire. For this reason in the (411) wire sample the maximum energy shift is about 14 meV when the piezoelectric field is completely screened. On the other hand, in the (111) quantum wires, despite the expected larger value of the piezoelectric potential occurring far from the centre, the stronger wave-function confinement in wire regions where the piezoelectric field is quite low, causes a maximum energy shift of only 5 meV. These theoretical results are in agreement with the density dependent screening induced energy shifts measured in figure 5. Let us note that the interface polarization charge densities seen by the wave functions in the two structures are 3.0×10^{11} cm^{-2} and 0.5×10^{11} cm^{-2} for the (411) and (111) wires, respectively. Consequently, in order to completely locally screen the piezoelectric fields we need to introduce in both wires areal charge densities of the order of 10^{11} cm^{-2}, consistent with our experiment (see figure 5(b)).

5. Conclusions

In conclusion we have investigated the time resolved optical non-linearity of strained InGaAs(111) and (411) V-shaped QWRs. The screening of the internal piezoelectric field by the photo-generated carrier density has been temporally resolved by measuring the QWRs PL shift for increasing delays after the laser pulse (blue-shift in the early 150 ps, and the recovery of the unscreening level afterward). The value of the energy shift strongly depends on the excitation carrier density, and on the direction of the groove sidewalls. The experimental values of the energy shift are consistent with the theoretical calculation of the polarization charge density induced by the piezoelectric field and with the associated piezoelectric potential across the wire profile.

Acknowledgments

We gratefully acknowledge the expert technical help of D Cannoletta, A Melcarne, A Miccoli and C Blasi. We thank Dr G Colì, for stimulating and helpful discussions. This work has been supported by: (i) Progetto Sud INFM: quantum wires V-groove for opto-electronic applications; (ii) TMR European Research Network: ultrafast quantum optoelectronics. One of the authors (AT) gratefully acknowledges support from the EU.

References

[1] Nye J 1985 *Properties of Crystals* (Oxford: Oxford University Press)
[2] Vaccaro P O, Takahashi M, Fujita K and Watanabe T 1995 *Japan. J. Appl. Phys.* **34** L13
[3] Vaccaro P O, Tominaga K, Hosoda M, Fujita K and Watanabe T 1995 *Japan. J. Appl. Phys.* **34** 1362
[4] Hogg R A, Fisher T A, Willcox A R K, Whittaker D M, Skolnick M S, Mowbray D J, David J P R, Pabla A S, Rees G J, Grey R, Woodhead J, Sanchez-Rojas J L, Hill G, Pate M A and Robson P N 1993 *Phys. Rev.* B **48** 8491
[5] Campbell I H, Joswick M D and Smith D L 1995 *Appl. Phys. Lett.* **66** 988
[6] Vaccaro P O, Hosoda M, Fujita K and Watanabe T 1996 *Japan. J. Appl. Phys.* **3** 1292
[7] Cartwright A N, McCallum D S, Boggess T F, Smirl A L, Moise T S, Guido L J, Barker R C and Wherrett B S 1993 *J. Appl. Phys.* **73** 7767
[8] Sánchez-Rojas J L, Sacedón A, Calleja E, Muñoz E, Sanz-Hervas A, De Benito G and Lopez M 1996 *Phys. Rev.* B **53** 15 469
[9] Harken D R, Huang X R, McCallum D S, Smirl A L, Sánchez-Rojas J L, Sacedón A, Calleja E and Muñoz E 1995 *Appl. Phys. Lett.* **66** 857
[10] Huang X R, Harken D R, Cartwright A N, Smirl A L, Sánchez-Rojas J L, Sacedón A, Calleja E and Muñoz E 1995 *Appl. Phys. Lett.* **67** 950
[11] Rinaldi R, Cingolani R, Lepore M, Ferrara M, Catalano I M, Rossi F, Rota L, Molinari E, Lugli P, Marti U, Martin D, Morier-Gemoud F, Ruterana P and Reinhart F K 1994 *Phys. Rev. Lett.* **73** 2899
[12] Rossi F, Molinari E, Rinaldi R and Cingolani R 1996 *Solid State Electron.* **40** 249
[13] Rinaldi R, Cingolani R, De Caro L, Lomascolo M, Di Dio M, Tapfer L, Marti U and Reinhart F K 1996 *J. Opt. Soc. Am.* B **13** 1031
[14] Cingolani R, Rinaldi R, Lomascolo M, Colì G, Passaseo A, Emiliani V, De Vittorio M 1997 *Nonlin. Opt.* **18** 347
[15] Ilg M, Heberle A and Ploog K 1994 *Solid State Electron.* **37** 739
[16] Nötzel R, Ramsteiner M, Niu Z, Schönherr H P, Däweritz L and Ploog K *Appl. Phys. Lett.* **70** 1578
[17] Sale T E, Woodhead J, Rees G J, Grey R, David J P R, Pabla A S, Rodriguez-Girones P J, Robson P N, Hogg R A and Skolnik S 1994 *J. Appl. Phys.* **76** 5447
[18] For the calculation of the (411) QW eigenstates, the strain has been linearly interpolated between the strain of the (100) QW and of the (111) QW as a function of the angle between the sidewalls QW and the (100) crystallographic plane.
[19] Lomascolo M, Ciccarese P, Rinaldi R, Cingolani R and Reinhart F K 1998 *J. Appl. Phys.* **83** 302
[20] De Caro L and Tapfer L 1993 *Phys. Rev.* B **48** 2298
[21] De Caro L and Tapfer L 1996 *J. Appl. Phys.* **79** 9188